TISSUE ENGINEERING: Part A
Volume 24, Numbers 13 and 14, 2018

DOI: 10.1089/ten.tea.2017.0297

termis
Tissue Engineering
& Regenerative Medicine
International Society

ORIGINAL ARTICLE

Mineralized Biomaterials Mediated Repair of Bone Defects Through Endogenous Cells

Eva C. González Díaz, BS,[1,*] Yu-Ru V. Shih, PhD,[1,†,*] Manando Nakasaki, PhD,[1] Mengqian Liu, MS,[1,2,‡] and Shyni Varghese, PhD[1,2,†,‡,§]

Synthetic biomaterials that create a dynamic calcium (Ca^{2+})-, phosphate (PO_4^{3-}) ion-, and calcium phosphate (CaP)-rich microenvironment, similar to that found in native bone tissue, have been shown to promote osteogenic commitment of stem cells *in vitro* and *in vivo*. The intrinsic osteoconductivity and osteoinductivity of such biomaterials make them promising bone grafts for the treatment of bone defects. We thus aimed to evaluate the potential of mineralized biomaterials to induce bone repair of a critical-sized cranial defect in the absence of exogenous cells and growth factors. Our results demonstrate that the mineralized biomaterial alone can support complete bone formation within critical-sized bone defects through recruitment of endogenous cells and neo-bone tissue formation in mice. The newly formed bone tissue recapitulated many key characteristics of native bone such as formation of bone minerals reaching similar bone mineral density, presence of bone-forming osteoblasts and tartrate-resistant acid phosphatase-expressing osteoclasts, as well as vascular networks. Biomaterials that recruit endogenous cells and provide a tissue-specific microenvironment to modulate cellular behavior and support generation of functional tissues are a key step forward in moving bench-side tissue engineering approaches to the bedside. Such tissue engineering strategies could eventually pave the path toward readily available therapies that significantly reduce patient cost of care and improve overall clinical outcomes.

Keywords: mineralized biomaterial, critical defect, bone repair, osteoinductive

Introduction

Bone is a highly dynamic tissue with an intrinsic ability to regenerate or repair in response to traumatic injury. Despite this regenerative ability, extensive bone loss due to severe trauma, infection, tumor excision, and degenerative disease may lead to bone defects that often require surgical intervention and the use of bone grafts to assist healing. In the United States alone, ~1.6 million bone grafts are needed on an annual basis, resulting in a cost of over 27 billion dollars.[1] For decades, autografts and allografts have remained the standard of care for the treatment of non-healing bone defects.[2] These methodologies, however, suffer from major drawbacks such as donor site morbidity and pain, scarcity, immunorejection, and risk of disease transmission.[2–4] In addition, a secondary surgery is required for graft harvest, increasing the cost of care and lengthening the treatment process.

Recent efforts have thus focused on developing alternative treatment strategies like tissue engineering, wherein a biomaterial is used in conjunction with exogenous cells or osteoinductive growth factors, such as bone morphogenetic proteins (BMPs).[5,6] Although these biological-dependent therapies have shown great efficacy in promoting bone regeneration, they suffer from numerous drawbacks. The use of high BMP doses to expedite bone formation has been correlated with an increased risk of tumorigenesis and other side effects, such as local bone resorption and ectopic bone formation.[7,8] In addition, the effectiveness of exogenous cell-based therapies is often limited by their scarcity and heterogeneity.[9,10] Biomaterials that possess intrinsic osteoconductivity, osteoinductivity, and osteogenicity and exploit the bone-forming potential of endogenous cells could provide a widely accessible method for treating critical bone defects.

We have recently developed a biomineralization strategy to create mineralized biomaterials capable of modulating

Departments of [1]Bioengineering and [2]Materials Science and Engineering, University of California, San Diego, La Jolla, California.
[†]*Current affiliation:* Department of Orthopaedic Surgery, Duke University, Durham, North Carolina.
[‡]*Current affiliation:* Department of Mechanical Engineering and Materials Science, Duke University, Durham, North Carolina.
[§]*Current affiliation:* Department of Biomedical Engineering, Duke University, Durham, North Carolina.
*These two authors contributed equally to this work.

extracellular concentrations of calcium (Ca^{2+}) and phosphate (PO_4^{3-}) ions to successfully recapitulate the dynamic extracellular mineral environment of native bone tissues.[11] Our studies have shown that these biomineralized matrices induce osteogenic differentiation of stem cells, including mesenchymal stem cells, embryonic stem cells, and induced human pluripotent stem cells, even in the absence of other osteoinductive molecules[12–16] and support bone tissue formation and donor bone marrow cells *in vivo*.[17–19] In this study, we evaluated the potential of these biomineralized scaffolds to direct orthotopic bone formation in a critical-sized cranial defect in mice. We demonstrate that treatment with these mineralized biomaterials results in bone formation of the defect through the formation of mature, vascularized bone tissues from recruited host cells.

Materials and Methods

Graft synthesis and mineralization

Macroporous poly(ethylene glycol)-diacrylate-co-N-acryloyl 6-aminocaproic acid (PEGDA-co-A6ACA) hydrogels were prepared by using a cryogelation method detailed previously.[20] PEGDA and A6ACA were synthesized as described elsewhere.[21,22] A precursor solution consisting of 20% (w/v) PEGDA ($M_n = 3.4$ kDa) and 0.5 M A6ACA were prepared in 0.5 M NaOH. The precursor solution was mixed with 0.5% (w/v) ammonium persulfate and 0.2% (v/v) N, N, N′-N′-tetramethylethylenediamine (TEMED). Approximately 75 μL of the above solution was placed onto a chilled polystyrene dish. A chilled 15 mm coverslip was placed over the precursor solution and the solution was left to polymerize for 24 h at −20°C. Phosphate-buffered solution (PBS) maintained at room temperature was added to the gel to thaw ice crystals within the crosslinked structures and form macroporous hydrogels. The macroporous hydrogels (i.e., cryogels) were subsequently punched into 4 mm diameter disks of 0.7 mm thickness.

Mineralization of the cryogels was achieved by immersing the structures in simulated body fluid (m-SBF), prepared as previously described,[11] for 12 h, and subsequently in 40 mM Ca^{2+}/24 mM PO_4^{3-} (pH 5.2) under vacuum for 1 h. The cryogels were briefly rinsed in ultrapure water and immersed in fresh m-SBF for 48 h at 37°C. The mineralized cryogels were then briefly washed with PBS to remove excess m-SBF, sterilized by immersion in 70% ethanol for 3 h, and washed in sterile PBS.

Scanning electron microscopy and energy-dispersive spectra

Scanning electron microscopy (SEM) was used to examine the pore structures of non-mineralized and mineralized cryogels. Cryogels from each group were sliced into thin pieces and lyophilized for 24 h. These samples were then sputter coated (Emitech, K575X) with iridium for 7 s and imaged using SEM (Philips XL30 ESEM). The mineral composition of the mineralized cryogels was determined through energy-dispersive spectra (EDS) analysis. ICA software was used to quantify the calcium to phosphate atomic ratio (Ca/P) from the resulting elemental spectra.

Surgical procedure and biomaterial implantation

In vivo function of the implants was performed in C57BL6/J mice (2 months old) following the approval of the Institutional Animal Care and Use Committee (IACUC) at the University of California, San Diego, and was performed in accordance with national and international guidelines for laboratory animal care. Prior to surgery, mice were anesthetized using ketamine (Ketaset, 100 mg/kg) and xylazine (AnaSed, 10 mg/kg) buprenorphine (0.05 mg/kg) through intraperitoneal injection. A skin incision was made along the length of the calvaria to expose the parietal region and a 4 mm diameter defect was made in both the left and right parietal bones with a 4 mm biopsy punch.[23] A sterile cryogel (mineralized and non-mineralized) was transplanted onto each defect site. Following implantation, the skin was sutured and mice were kept on a warm heating pad until wakening. Mice were kept in separate housing cages. The ability of the mineralized biomaterials to support neo-bone tissue formation to repair critical bone defects was compared against groups treated with corresponding non-mineralized materials and groups with sham surgeries (untreated defects). The bone tissue formation and healing of the critical bone defects were analyzed as a function of time at 2 and 8 weeks postprocedure.

Microcomputed tomography

Microcomputed tomography (μCT) was performed to assess hard tissue formation within the cranial defects at 2 and 8 weeks postimplantation. All the groups (Sham, treated with non-mineralized and mineralized implants) were also imaged immediately after the implantation (termed as week 0 in Fig. 2A). The entire skull of each mouse was harvested and fixed in 4% paraformaldehyde for 4 days at 4°C. Samples were rinsed with PBS and secured tightly between styrofoam disks within a conical tube. Scanning was performed using SkyScan 1076 (Bruker: 9 μm pixel, 50 kV, 0.5 mm Al filter). Scan reconstruction was performed using NRecon software (SkyScan; Bruker). Using CT Analyser software (SkyScan; Bruker), bone structures were segmented using a threshold of 95–255. Bone mineral density (bone volume/total volume, BV/TV) was quantified within the bone defect site. Three-dimensional (3D) models were generated using CT Analyser and rendered in CT Volume software (SkyScan; Bruker). Defect closure was quantified by running the 3D models through the particle analysis function on ImageJ.

Histology and immunohistological staining

Excised samples were first decalcified using 10% ethylenediaminetetracetic acid (EDTA, pH 7.3) for 2 weeks at 4°C and rinsed with PBS. The samples were then gradually dehydrated using increasing concentrations of ethanol and incubated in Citrisolv until equilibrium was reached. Following dehydration, samples were immersed in a mixture of 50% (v/v) Citrisolv, 47.5% (w/w) Paraffin, and 2.5% (w/w) poly (ethylene-co-vinyl acetate) (437220; Sigma) for 30 min at 70°C.

Hematoxylin and eosin (H&E) staining was performed on rehydrated sections by first incubating the samples in hematoxylin solution (catalog no. 3536-16; Ricca) for 1 min and rinsing with ultrapure water. The samples were then incubated with Eosin-Y solution (catalog no. 7111; Richard-Allan Scientific) for 45 s and rinsed with ultrapure water. Stained sections were gradually dehydrated using increasing concentrations of ethanol and immersed in Citrisolv until equilibrium

was reached. Sections were mounted in glycerol and imaged using a Keyence microscope (BZ-X700).

Tartrate-resistant acid phosphatase (TRAP) staining was performed by following the manufacturer's instructions (catalog no. 387A; Acid Phosphatase Kit, Sigma-Aldrich).[23] The solution was prepared by first mixing 50 μL of Fast Garnet GBC base solution with 50 μL of sodium nitrite solution. This mixture was added to 4.5 mL of prewarmed DI water at 37°C. After mixing, 50 μL of Naphthol AS-B1 phosphate solution, 200 μL of acetate solution, and 100 μL of tartrate solution were added to the solution and mixed to generate a working solution. Rehydrated sections were immersed in the working solution, incubated at 37°C for 1 h covered from light, and rinsed with ultrapure water. Sections were then gradually dehydrated using increasing concentrations of ethanol and immersed in Citrisolv until equilibrium was reached. Slides were mounted with glycerol and imaged immediately.

For immunohistochemical and immunofluorescent staining, rehydrated sections were immersed in a solution of proteinase K (20 μg/mL, catalog no. 1000005393; Invitrogen) in 95% (v/v) TE buffer (50 mM Tris-HCl, 1 mM EDTA, and 0.5% [v/v] Triton X-100; pH 8) with 5% (v/v) glycerol and incubated for 15 min at 37°C. For immunohistochemical staining, sections were incubated in a blocking solution containing 3% (w/v) bovine serum albumin (BSA) and 5% normal serum for 1 h at 25°C. Samples were incubated in primary antibody against osteocalcin (1:100, rabbit polyclonal, catalog no. 1000005393; Abcam), RANK (1:200, mouse monoclonal, catalog no. ab13918; Abcam), and BMP2 (catalog no. ab14933, 1:500, rabbit polyclonal; Abcam) in a blocking solution for 9 h at 4°C. For RANK staining, a mouse on mouse (M.O.M) immunodetection kit (Vector laboratories) was used. Sections were rinsed in PBS and treated with 3% (v/v) hydrogen peroxide for 7 min at 25°C. The samples were then incubated with secondary antibody (1:100, horseradish peroxidase-conjugated donkey anti-rabbit, catalog no. 711-035-152; Jackson ImmunoResearch) in a blocking solution for 1 h at 25°C. Sections were rinsed in PBS and developed by immersion in 3-3′ diaminobenzidine (DAB)

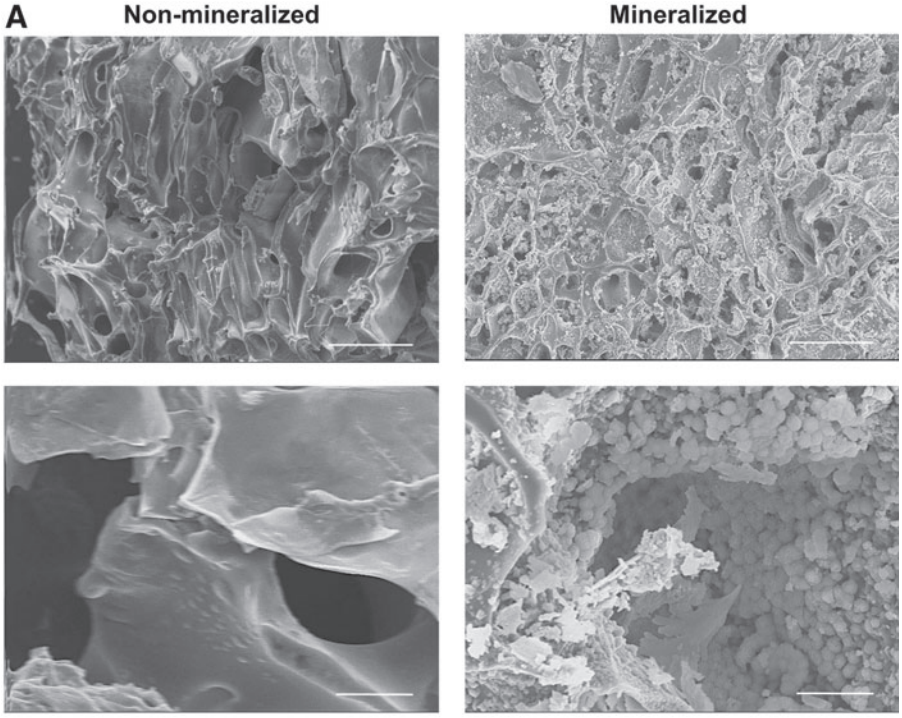

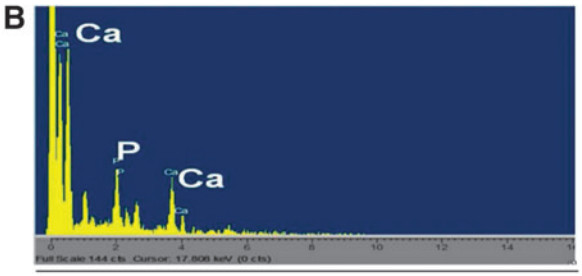

Element	Weight%	Atomic%
P	34.04	40.04
Ca	65.96	59.96
Totals	100.00	100.00

FIG. 1. Biomineralized matrix characterization. **(A)** SEM images of non-mineralized and mineralized macroporous cryogels. Scale bars: 100 μm (*top panels*) and 10 μm (*lower panels*). **(B)** EDS showing presence of calcium and phosphate ions within mineralized hydrogels. EDS, energy-dispersive spectra; SEM, scanning electron microscopy. Color images available online at www.liebertpub.com/tea

substrate solution (catalog no. SK-4100; Vector Laboratories) for 2 min at 25°C. The developed sections were washed with PBS and gradually dehydrated using increasing concentrations of ethanol and immersed in Citrisolv until equilibrium was reached. Slides were mounted in glycerol and imaged immediately. For immunofluorescent staining, sections were washed with PBS and permeabilized using 0.1% Triton X for 10 min at 25°C, which were then treated with sodium borohydride solution (2.5 mg/mL in 50% [v/v] ethanol) for 30 min at room temperature. The sections were immersed in a blocking solution (3% [w/v] BSA and 0.1% [v/v] Triton X) and incubated for 1 h at 25°C. Sections were then incubated with primary antibody against CD31 (Platelet endothelial cell adhesion molecule [PECAM-1], catalog no. sc-1506, 1:100; goat Santa Cruz Biotechnology) in a blocking solution for 12 h at 4°C and washed with PBS.

Statistical analyses

Statistical analyses were performed using a minimum of four samples for each experimental group. All experiments were repeated independently at least twice. Statistical analysis was performed using GraphPad Prism 6. Two-tailed Student's *t*-test was applied when comparing two groups within the same time point. One-way analysis of variance with Turkey-Kramer *post hoc* test was used for comparisons between multiple groups within the same time point.

Results

Characterization of mineralized biomaterials

The macroporous structure of non-mineralized and mineralized cryogels was confirmed through SEM (Fig. 1A). In addition to the interconnected macroporous structures, SEM imaging also revealed the presence of bound minerals within the mineralized matrices, which exhibited a flat, plate-shaped morphology (Fig. 1A). Elemental analysis further confirmed the presence of CaP minerals within the mineralized cryogels and the calcium (Ca^{2+}) to phosphate (PO_4^{3-}), (Ca/P), ratio was estimated to be 1.5 (Fig. 1B). We have previously demonstrated that the CaP minerals found within these mineralized biomaterials spontaneously undergo dissolution into $Ca^{2+}$and PO_4^{3-} ions.[12]

Evaluation of hard tissue formation using μCT

Hard tissue formation within the cranial defects treated with mineralized and non-mineralized cryogels, as well as sham groups, was examined by using μCT at 0, 2, and 8 weeks postimplantation (Fig. 2). As evident from the μCT images, the as-synthesized mineralized cryogels are not inherently radio-opaque. Two and 8 weeks postimplantation analysis showed further calcification of the implanted mineralized cryogels compared to non-mineralized and sham groups (Fig. 2A). Quantification of hard tissue formation in the defect site revealed a significantly higher BV in groups treated with mineralized cryogels compared to sham and non-mineralized groups. Furthermore, the percent BV at 8 weeks was comparable to that in the surrounding native bone tissue (Fig. 2B). In contrast, sham and non-mineralized groups revealed minimal to no hard tissue formation within the defect site throughout the extent of the study.

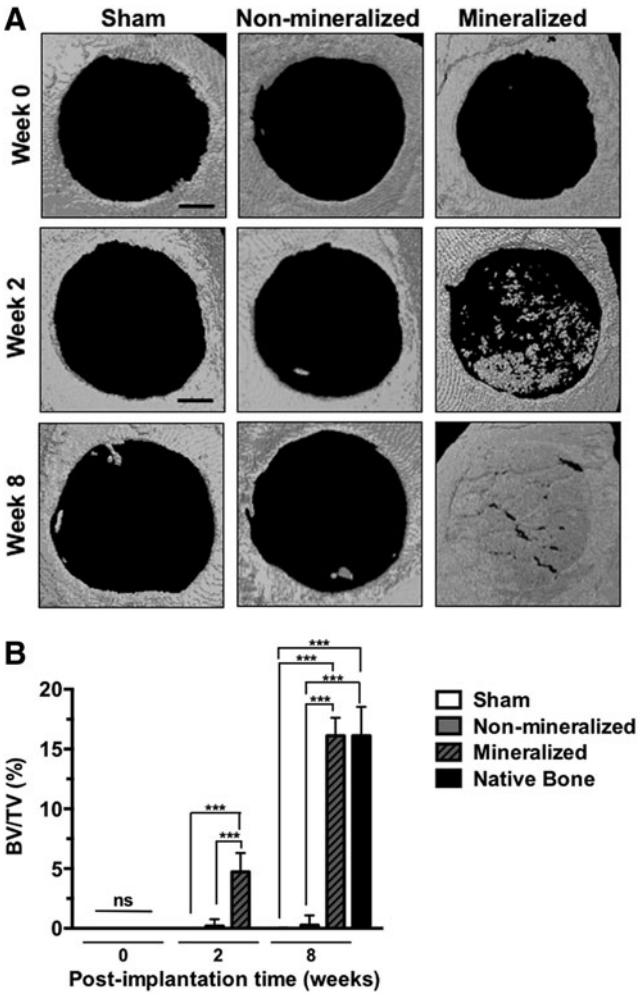

FIG. 2. Calcified bone tissue formation within critical-sized cranial defects. **(A)** μCT images of mouse cranial defects treated with mineralized and non-mineralized cryogels, as well as sham groups, at 0 (day 0), and 2 and 8 weeks postimplantation. Scale bars: 1 mm. **(B)** Quantification of bone volume for sham, non-mineralized, and mineralized groups at 2 and 8 weeks posttreatment. *Asterisks* denote *p* values with statistical significance (***$p < 0.001$). μCT, Microcomputed tomography.

Histological assessment of bone formation

H&E staining was performed for cranial sections harvested following 2 and 8 weeks posttreatment to further evaluate the healing process and neo-bone tissue formation at the defect site (Supplementary Figs. S1 and S3, respectively; Supplementary Data are available online at www.liebertpub.com/tea). After 2 weeks, defects treated with both non-mineralized and mineralized biomaterials showed significant host cell infiltration, which was homogeneously distributed throughout the implant (Supplementary Fig. S1). By 8 weeks, groups treated with mineralized cryogels revealed relatively higher extracellular matrix (ECM) content throughout the defect site compared to non-mineralized cryogels (Fig. 3). Despite significant host cell infiltration, no detectable hard tissue formation was observed in defects treated with non-mineralized cryogels even after 8 weeks. In the case of sham groups, no bone formation was observed and the defects were bridged by

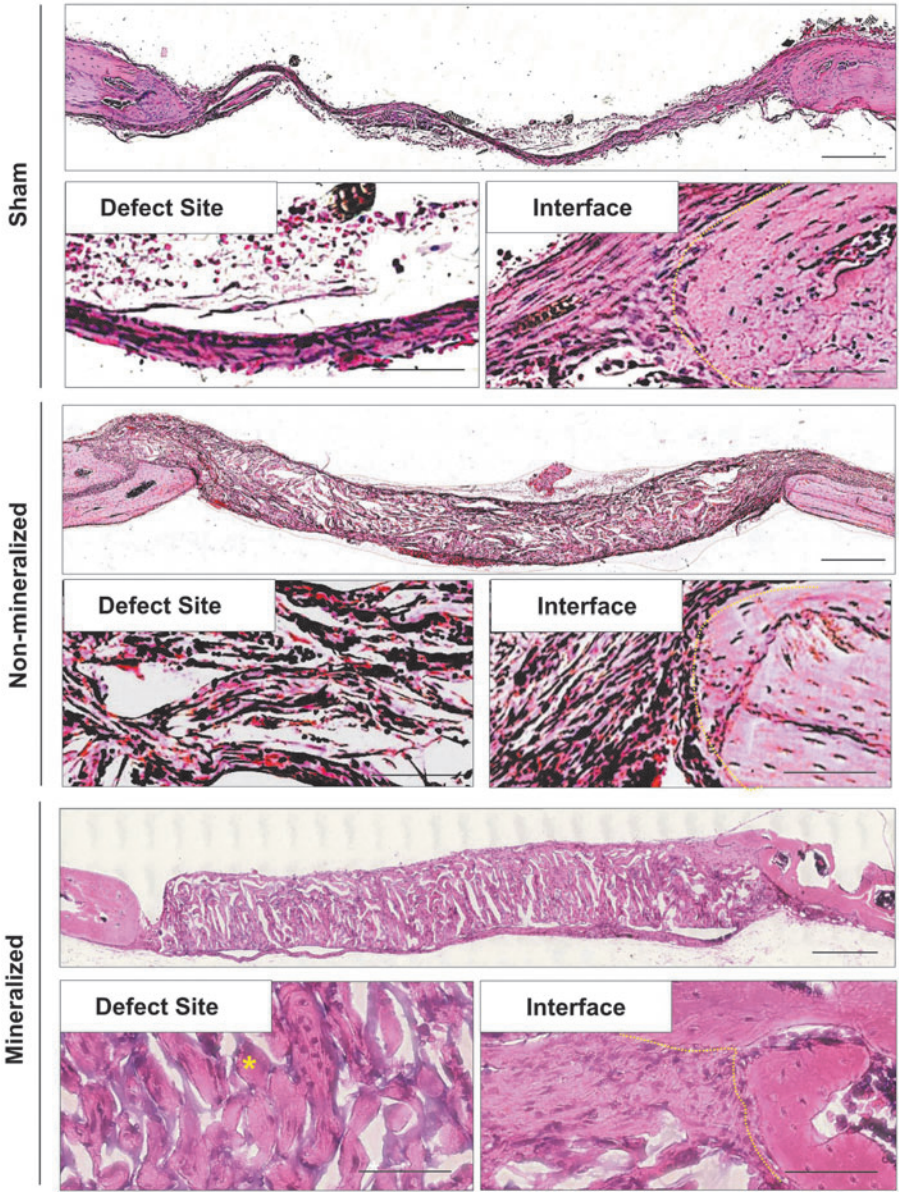

FIG. 3. Morphological assessment of bone formation within critical-sized cranial defects. H&E staining of cranial sections following 8 weeks of implantation. High magnification images reveal bone tissue within the defect site (*lower left panels*) and at the interface between the defect site and native bone (*lower right panels*). A *yellow dotted line* was used to delineate the location of the interface between the neo-tissue/implant and native bone. *Yellow asterisks* denote bone tissue. Scale bars: 500 μm (*upper panel*) and 20 μm (*lower panels*). H&E, hematoxylin and eosin. Color images available online at www.liebertpub.com/tea

a thin layer of fibrous tissue, which is consistent with that normally found in non-healing bone defects (Fig. 3 and Supplementary Fig. S1).[24]

Evaluation of bone-specific markers

To further confirm the bone tissue formation, the tissue sections were stained for osteocalcin, a bone-specific matrix protein that is secreted by osteoblasts (Fig. 4A, B and Supplementary Fig. S2A, B). At 2 weeks, groups treated with mineralized cryogels showed presence of ECM enriched with osteocalcin (Supplementary Fig. S2A, B). A similar finding was also observed after 8 weeks of postimplantation (Fig. 4A). These findings are further shown by histogram intensity of the images, in which lower histogram values indicate higher osteocalcin expression (Fig. 4B). In contrast, defects treated with non-mineralized cryogels showed minimal presence of osteocalcin at the defect site, at both 2 and 8 weeks postimplantation. The fibrous-like tissue bridging the defect site of sham groups was found to have some, but less, osteocalcin deposition at both 2 and 8 weeks posttreatment. After 2 weeks of implantation, the mineralized group, but not the sham and non-mineralized group, showed BMP2 expression, a protein commonly involved during osteogenesis (Fig. S2C, D).

TRAPstaining was performed to examine the presence of osteoclast-like cells within the neo-bone tissue (Fig. 4C, D and Supplementary Fig. S2E, F). TRAP-positive cells were detected in both the defects treated with mineralized and non-mineralized cryogels at 2 weeks postimplantation (Supplementary Fig. S2E, F). Following 8 weeks of treatment, an increase in TRAP-positive cells was observed in defects treated with mineralized cryogels, but none was detected for groups treated with non-mineralized cryogels (Fig. 4C). No TRAP-positive cells were observed for sham groups at both 2 and 8 weeks postprocedure. Quantification of TRAP staining at 8 weeks posttreatment corroborated

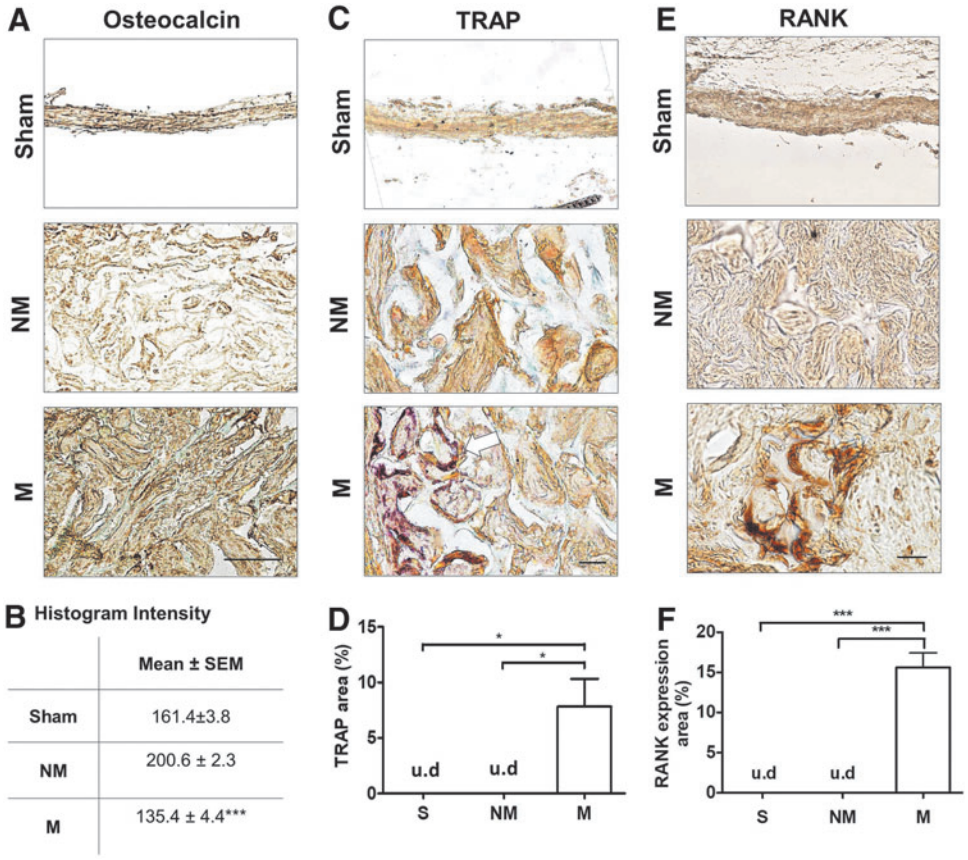

FIG. 4. Bone-specific markers in newly formed tissue within cranial defects. **(A)** Immunohistochemical staining of osteocalcin for sham (S), non-mineralized (NM), and mineralized (M) groups and **(B)** mean histogram intensity of images following 8 weeks of implantation. Lower intensity values correspond to higher expression. **(C)** Histochemical staining for TRAP and **(D)** percent positive area of the cranial defect site for sham (S), non-mineralized (NM), and mineralized (M) treatment groups following 8 weeks of implantation. *Arrow* indicates TRAP-positive cells found within the constructs. **(E)** Histochemical staining for RANK and **(F)** percent positive area of the cranial defect site for sham (S), non-mineralized (NM), and mineralized (M) treatment groups following 8 weeks of implantation. Scale bars: 30 μm. *Asterisks* denote p values with statistical significance ($*p<0.05$, $***p<0.001$). RANK, receptor activator of nuclear factor κB; TRAP, tartrate-resistant acid phosphatase; u.d, undetectable. Color images available online at www.liebertpub.com/tea

aforementioned observations (Fig. 4D). To further confirm the presence of osteoclasts, receptor activator of nuclear factor κB (RANK) expression, a marker of osteoclasts,[25] was positive in the mineralized, but not sham and non-mineralized groups after 2 weeks postimplantation (Fig. 4E, F).

Vascularization of implanted grafts

As evident from Supplementary Figure S1, the H&E staining of the tissue sections following 2 weeks of implantation showed vascular connections throughout the implant and at the defect interface with the native bone, suggesting formation of anastomosed vessels with the host. The formation of vasculature was further confirmed by staining for PECAM-1 (Fig. 5 and Supplementary Fig. S3). Groups treated with mineralized and non-mineralized macroporous matrices revealed the presence of PECAM-1-positive cells within the defect at 2 and 8 weeks postimplantation. In contrast, tissue sections of sham groups showed no evidence of vascularization throughout the defect site.

Discussion

In this study, we evaluated the potential of macroporous, mineralized biomaterials to stimulate bone healing in the absence of exogenous biologicals by using a critical-sized cranial defect as a model system. Results from our studies show that mineralized macroporous matrices promoted hard tissue formation that led to complete healing of the cranial defect by 8 weeks postimplantation. Histological analysis of the defects revealed extensive host cell infiltration within both non-mineralized and mineralized cryogels. This suggests that cell infiltration is a consequence of the macroporous nature of the scaffolds, which supported homogeneous distribution of the host cells throughout the implant. The μCT analyses along with the osteocalcin staining suggest that despite the widespread cell infiltration, only cells within the mineralized materials contributed to the formation of bone-forming cells and hard tissue formation, highlighting the importance of the mineral environment in promoting osteogenic differentiation of recruited cells, and to bone tissue formation. These *in vivo* findings are consistent with our *in vitro* findings, where we have

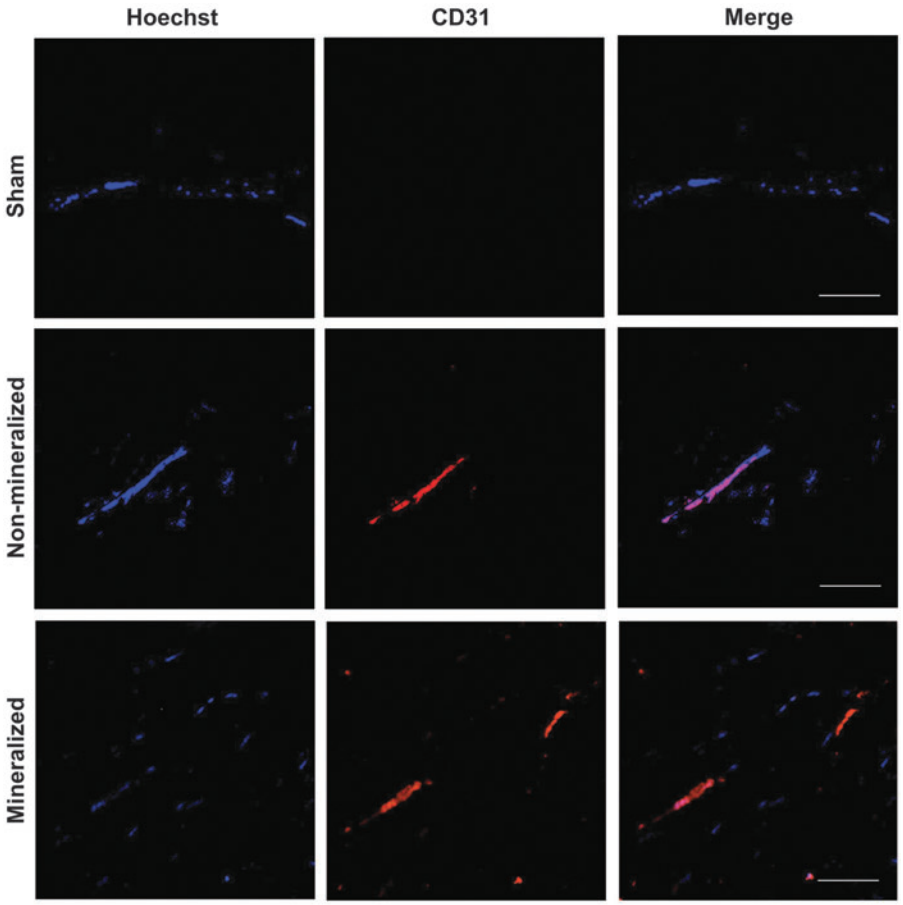

FIG. 5. Vascularization of mineralized constructs. Immunofluorescent staining for platelet endothelial cell adhesion molecule (CD31) and Hoechst 33342 staining of cell nuclei within the defect site for sham, non-mineralized, and mineralized treatment groups following 8 weeks of implantation. Scale bars: 100 μm. Color images available online at www.liebertpub.com/tea

demonstrated the importance of CaP minerals in directing osteogenic differentiation of stem cells.[12–15] We have also showed previously that these mineralized scaffolds when implanted in the subcutaneous space of a rat, recruited endogenous cells to form bone tissue.[17]

The physicochemical properties of the mineralized scaffold play a key role in supporting osteogenic differentiation of progenitor cells and bone tissue formation. For instance, previous studies have shown that the dissolution properties of calcium phosphate minerals could contribute to the osteoinductive ability of biomaterials. Higher osteoinductive potential was observed with scaffolds containing resorbable biphasic calcium phosphate and β-TCP compared to hydroxyapatite.[26–28] Recently, we have shown that the CaP minerals present in the mineralized materials readily dissociate into Ca^{2+} and PO_4^{3-} ions and modulate their concentration in the extracellular milieu.[13,29] Both extracellular Ca^{2+} and PO_4^{3-} play a key role in promoting osteogenic differentiation of stem cells.[13,30–34] In addition, the dissolution and precipitation of CaP minerals facilitate sequestration of angiogenic and osteoinductive growth factors, which further contribute to bone tissue formation.[35]

Combined and coordinated action of osteoblasts and osteoclasts is essential to maintain bone homeostasis. It is therefore necessary that engineered bone grafts provide a permissive environment for bone remodeling to take place. Although TRAP-positive cells were observed in defects treated with both mineralized and non-mineralized cryogels after 2 weeks treatment, their presence at 8 weeks was observed only in groups treated with mineralized cryogels. TRAP-positive cells detected in the non-mineralized groups at 2 weeks suggest that monocytic/osteoclast precursors possibly migrated from the surrounding bone[36] and contributed to TRAP positivity in the grafts, while the non-calcified environment lacking osteoblasts and their secreted factors does not support their continued activity at 8 weeks.[37,38] In addition to neo-bone tissue formation, successful healing of bone defects requires vascularization and anastomosis of the implant with the host tissue.[39,40] Our results demonstrate that the macroporous architecture of our scaffold facilitated the infiltration of host cells as well as vascularization of the implant. Prior studies have also shown the influence of bone-residing osteoblasts in angiogenesis by secreting vascular endothelial growth factor A.[41,42]

In summary, as the need to develop simple treatment strategies that are reliable and cost-effective has become increasingly important, the studies described here demonstrate that mineralized macroporous biomaterials alone are sufficient to promote the formation of functional bone tissue and achieve complete healing of bone defects. While the macroporous structure of the scaffold enabled infiltration of host cells, the osteogenic differentiation of recruited cells and maintenance of osteoblasts required the presence of mineral environment. The newly formed tissue, although appears to be immature at 8 weeks postimplantation time, recapitulated many key characteristics of native bone tissue such as presence of bone-forming osteoblasts and TRAP-expressing osteoclasts, as well as vascular networks. Such

approaches involving synthetic biomaterials that not only support bone formation but also facilitate vascularization solely by recruitment of host progenitors, without the need of exogenous donor cells and growth factors provide an attractive alternative to current therapeutic strategies involving osteoinductive growth factors and bone tissue derivatives.

Conclusions

Studies described in this work demonstrate the ability of mineralized, macroporous biomaterials to direct bone healing of critical-sized cranial defects. By providing a bone-specific mineral environment, these biomaterials induce osteogenic commitment of recruited host progenitor cells and support the maintenance of cells relevant for the formation and function of bone tissues, including vascularization of the implant during repair. Development and optimization of biomaterials to harness the regeneration potential of host tissue by activating endogenous cells to treat critical bone defects provide a step forward in advancing tissue engineering-based approaches for the treatment of critical bone defects. Such biomaterial-based strategies provide an effective and easy-to-implement alternative for bone tissue regenerative therapy.

Acknowledgment

The authors acknowledge the financial support from National Institutes of Health (NIH, Grant 1 R01 AR063184).

Disclosure Statement

No competing financial interests exist.

References

1. O'Keefe, R.J., and Mao, J. Bone tissue engineering and regeneration: from discovery to the clinic—an overview. Tissue Eng Part B Rev **17,** 389, 2011.
2. Giannoudis, P.V., Dinopoulos, H., and Tsiridis, E. Bone substitutes: an update. Injury **36,** 20, 2005.
3. Lichte, P., Pape, H.C., Pufe, T., Kobbe, P., and Fischer, H. Scaffolds for bone healing: concepts, materials and evidence. Injury **42,** 569, 2011.
4. Laurie, S.W.S., Kaban, L.B., Mulliken, J.B., and Murray, J.E. Donor-site morbidity after harvesting rib and iliac bone. Plast Reconstr Surg **73,** 933, 1984.
5. Zlotolow, D.A., Vaccaro, A.R., Salamon, M.L., and Albert, T.J. The role of human bone morphogenetic proteins in spinal fusion. J Am Acad Orthop Surg **8,** 3, 2000.
6. Khan, S.N., Fraser, J.F., Sandhu, H.S., Cammisa, F.P., Girardi, F.P., and Lane, J.M. Use of osteopromotive growth factors, demineralized bone matrix, and ceramics to enhance spinal fusion. J Am Acad Orthop Surg **13,** 129, 2005.
7. Carragee, E.J., Chu, G., Rohatgi, R., *et al.* Cancer risk after use of recombinant bone morphogenetic protein-2 for spinal arthrodesis. J Bone Joint Surg Am **95a,** 1537, 2013.
8. Lad, S.P., Bagley, J.H., Karikari, I.O., *et al.* Cancer after spinal fusion: the role of bone morphogenetic protein. Neurosurgery **73,** 440, 2013.
9. Lepperdinger, G., Brunauer, R., Gassner, R., Jamnig, A., Kloss, F., and Laschober, G.T. Changes of the functional capacity of mesenchymal stem cells due to aging or age-associated disease—implications for clinical applications and donor recruitment. Transfus Med Hemother **35,** 299, 2008.
10. Moerman, E.J., Teng, K., Lipschitz, D.A., and Lecka-Czernik, B. Aging activates adipogenic and suppresses osteogenic programs in mesenchymal marrow stroma/stem cells: the role of PPAR-gamma2 transcription factor and TGF-beta/BMP signaling pathways. Aging Cell **3,** 379, 2004.
11. Phadke, A., Zhang, C., Hwang, Y., Vecchio, K., and Varghese, S. Templated mineralization of synthetic hydrogels for bone-like composite materials: role of matrix hydrophobicity. Biomacromolecules **11,** 2060, 2010.
12. Phadke, A., Shih, Y.R., and Varghese, S. Mineralized synthetic matrices as an instructive microenvironment for osteogenic differentiation of human mesenchymal stem cells. Macromol Biosci **12,** 1022, 2012.
13. Shih, Y.R., Hwang, Y., Phadke, A., *et al.* Calcium phosphate-bearing matrices induce osteogenic differentiation of stem cells through adenosine signaling. Proc Natl Acad Sci U S A **111,** 990, 2014.
14. Kang, H., Shih, Y.R., Hwang, Y., *et al.* Mineralized gelatin methacrylate-based matrices induce osteogenic differentiation of human induced pluripotent stem cells. Acta Biomater **10,** 4961, 2014.
15. Kang, H., Wen, C., Hwang, Y., *et al.* Biomineralized matrix-assisted osteogenic differentiation of human embryonic stem cells. J Mater Chem B **2,** 5676, 2014.
16. Wen, C., Kang, H., Shih, Y.R., Hwang, Y., and Varghese, S. In vivo comparison of biomineralized scaffold-directed osteogenic differentiation of human embryonic and mesenchymal stem cells. Drug Deliv Transl Res **6,** 121, 2016.
17. Phadke, A., Hwang, Y., Kim, S.H., *et al.* Effect of scaffold microarchitecture on osteogenic differentiation of human mesenchymal stem cells. Eur Cell Mater **25,** 114, 2013.
18. Shih, Y.R., Phadke, A., Yamaguchi, T., *et al.* Synthetic bone mimetic matrix-mediated in situ bone tissue formation through host cell recruitment. Acta Biomater **19,** 1, 2015.
19. Shih, Y.R., Kang, H., Rao, V., Chiu, Y.J., Kwon, S.K., and Varghese, S. In vivo engineering of bone tissues with hematopoietic functions and mixed chimerism. Proc Natl Acad Sci U S A **114,** 5419, 2017.
20. Hwang, Y., Sangaj, N., and Varghese, S. Interconnected macroporous poly(ethylene glycol) cryogels as a cell scaffold for cartilage tissue engineering. Tissue Eng Part A **16,** 3033, 2010.
21. Varghese, S., Lele, A., and Mashelkar, R. Metal-ion-mediated healing of gels. J Polym Sci Part A**44,** 666, 2005.
22. Zhang, C., Aung, A., Liao, L.Q., and Varghese, S. A novel single precursor-based biodegradable hydrogel with enhanced mechanical properties. Soft Matter **5,** 3831, 2009.
23. Kang, H., Shih, Y.R., Nakasaki, M., Kabra, H., and Varghese, S. Small molecule-driven direct conversion of human pluripotent stem cells into functional osteoblasts. Sci Adv **2,** e1600691, 2016.
24. Montjovent, M.O., Mathieu, L., Schmoekel, H., *et al.* Repair of critical size defects in the rat cranium using ceramic-reinforced PLA scaffolds obtained by supercritical gas foaming. J Biomed Mater Res A **83a,** 41, 2007.
25. Miron, R.J., Zohdi, H., Fujioka-Kobayashi, M., and Bosshardt, D.D. Giant cells around bone biomaterials: osteoclasts or multi-nucleated giant cells? Acta Biomater **46,** 15, 2016.
26. Habibovic, P., Yuan, H.P., van der Valk, C.M., Meijer, G., van Blitterswijk, C.A., and de Groot, K. 3D microenvironment

as essential element for osteoinduction by biomaterials. Biomaterials **26,** 3565, 2005.
27. Yuan, H., van Blitterswijk, C.A., de Groot, K., and de Bruijn, J.D. A comparison of bone formation in biphasic calcium phosphate (BCP) and hydroxyapatite (HA) implanted in muscle and bone of dogs at different time periods. J Biomed Mater Res A **78a,** 139, 2006.
28. Yuan, H.P., Van Blitterswijk, C.A., De Groot, K., and De Bruijn, J.D. Cross-species comparison of ectopic bone formation in biphasic calcium phosphate (BCP) and hydroxyapatite (HA) scaffolds. Tissue Eng **12,** 1607, 2006.
29. Kang, H., Shih, Y.R.V., and Varghese, S. Biomineralized matrices dominate soluble cues to direct osteogenic differentiation of human mesenchymal stem cells through adenosine signaling. Biomacromolecules **16,** 1050, 2015.
30. Suzuki, A., Ghayor, C., Guicheux, J., *et al.* Enhanced expression of the inorganic phosphate transporter Pit-1 is involved in BMP-2-induced matrix mineralization in osteoblast-like cells. J Bone Miner Res **21,** 674, 2006.
31. Cowan, C.M., Zhang, X.L., James, A.W., *et al.* NELL-1 increases pre-osteoblast mineralization using both phosphate transporter Pit1 and Pit2. Biochem Bioph Res Commun **422,** 351, 2012.
32. Beck, G.R. Inorganic phosphate as a signaling molecule in osteoblast differentiation. J Cell Biochem **90,** 234, 2003.
33. Wen, L., Wang, Y., Wang, H., *et al.* L-type calcium channels play a crucial role in the proliferation and osteogenic differentiation of bone marrow mesenchymal stem cells. Biochem Bioph Res Commun **424,** 439, 2012.
34. Zayzafoon, M. Calcium/calmodulin signaling controls osteoblast growth and differentiation. J Cell Biochem **97,** 56, 2006.
35. Lee, J.S., Suarez-Gonzalez, D., and Murphy, W.L. Mineral coatings for temporally controlled delivery of multiple proteins. Adv Mater **23,** 4279, 2011.
36. Nevius, E., Pinho, F., Dhodapkar, M., *et al.* Oxysterols and EBI2 promote osteoclast precursor migration to bone surfaces and regulate bone mass homeostasis. J Exp Med **212,** 1931, 2015.
37. Lacey, D.L., Tan, H.L., Lu, J., *et al.* Osteoprotegerin ligand modulates murine osteoclast survival in vitro and in vivo. Am J Pathol **157,** 435, 2000.
38. Udagawa, N., Takahashi, N., Jimi, E., *et al.* Osteoblasts/stromal cells stimulate osteoclast activation through expression of osteoclast differentiation factor/RANKL but not macrophage colony-stimulating factor: receptor activator of NF-kappa B ligand. Bone **25,** 517, 1999.
39. Patel, Z.S., Young, S., Tabata, Y., Jansen, J.A., Wong, M.E.K., and Mikos, A.G. Dual delivery of an angiogenic and an osteogenic growth factor for bone regeneration in a critical size defect model. Bone **43,** 931, 2008.
40. Aronin, C.E.P., Sefcik, L.S., Tholpady, S.S., *et al.* FTY720 promotes local microvascular network formation and regeneration of cranial bone defects. Tissue Eng Part A **16,** 1801, 2010.
41. Furumatsu, T., Shen, Z.N., Kawai, A., *et al.* Vascular endothelial growth factor principally acts as the main angiogenic factor in the early stage of human osteoblastogenesis. J Biochem **133,** 633, 2003.
42. Steinbrech, D.S., Mehrara, B.J., Saadeh, P.B., *et al.* Hypoxia regulates VEGF expression and cellular proliferation by osteoblasts in vitro. Plast Reconstr Surg **104,** 738, 1999.

Address correspondence to:
Shyni Varghese, PhD
Department of Biomedical Engineering, Mechanical Engineering & Materials Science, and Orthopaedics
Duke University, Durham
North Carolina

E-mail: shyni.varghese@duke.edu

Received: June 16, 2017
Accepted: January 22, 2018
Online Publication Date: March 23, 2018